ADVANCED FUNCTIONAL MATERIALS
www.afm-journal.de

Temperature Tunable 4D Polymeric Photonic Crystals

*Isabella De Bellis, Daniele Martella, Camilla Parmeggiani, Diederik Sybolt Wiersma, and Sara Nocentini**

Photonic crystals owe their multitude of optical properties to the way their structure creates interference effects. It is therefore possible to influence the photonic response by acting on their physical structure. In this article, tunable photonic crystals made by elastic polymers that respond to their environment are explored, in particular with a physical deformation under temperature variation. This creates a feedback process in which the photonic response depends on its physical structure, which itself is influenced by the environmental changes. By using a multi-photon polymerization process specifically optimized for soft responsive polymers such as Liquid Crystalline Networks, highly resolved, reproducible, and mechanically self-standing photonic crystals are fabricated. The physical structure of the 3D woodpile can be tuned by an external temperature variation creating a reversible spectral tuning of 50 nm in the telecom wavelength range. By comparing these results with finite element calculations and temperature induced shape-change, it is confirmed that the observed tuning is due to an elastic deformation of the structure. The achieved nanometric patterning of tunable anisotropic photonic materials will further foster the development of reconfigurable photonic crystals with point defects acting as tunable resonant cavities and, more in general, of 4D nanostructures.

1. Introduction

3D nano-structuration of smart materials makes miniaturized devices capable of responding to external stimuli.[1–6] These so-called 4D microstructures can exhibit a temporal evolution of their 3D shapes depending on the environmental conditions. To date, spatio-temporal control is mainly exploited for milli and micrometer structures while scaling these properties at the nanoscale is still an open challenge. At the same time, the possibility of developing programmable nano-voxels, achieving a dynamic control on the nano/micro (hierarchical) structures, would open to important breakthroughs in soft nanotechnology, such as in bio-medicine and tissue engineering,[7–10] nanophotonics,[11,12] nanoelectronics,[13,14] and nanorobotics[15] (**Figure 1**a). In these fields, responsive 3D nanostructures can be employed as stimuli-responsive actuators or tunable devices. In the first case, the polymer deformation can trigger autonomous movements and enable tasks at a length scale where other controls are not applicable,[16–18] while the latter exploits nanometric variations of the geometries for precise optical and electronic sensors.[4,19]

In this work, we demonstrated the spatio-temporal control of 3D printed photonic nanostructures whose 4D modulation can also be applied in all the above mentioned nanotechnology fields.

3D responsive photonic structures are mainly based on two fabrication strategies that rely on either self-assembly processes, a fast parallel manufacturing over large areas (as in case of opals),[20–24] or on deterministic printing processes via a two-photon absorption polymerization process (also called two-photon direct laser writing, TP-DLW) of sensitive polymers. The TP-DLW technique, being based on a nonlinear process, enables the point-by-point solidification of a liquid resin into 3D functional polymeric microstructures with features down to 150 nm. The combination of the material responsiveness and the nano-patterning with arbitrary designs, allows for an optical response that can be controlled in the 3D space by appropriate design, as well as over time by the local tuning of the material properties.

Polymers used for 3D responsive photonic structures should possess a good printability with TP-DLW and ensure reversible tuning of the optical properties. Remarkable examples include

I. De Bellis, D. Martella, C. Parmeggiani, D. S. Wiersma, S. Nocentini
European Laboratory for Nonlinear Spectroscopy
LENS
Via N. Carrara 1, Sesto Fiorentino, 50019 Firenze, Italy
E-mail: s.nocentini@inrim.it

D. Martella, D. S. Wiersma, S. Nocentini
National Institute of Metrological Research
INRiM
Strada delle Cacce 91, 10135 Torino, Italy

C. Parmeggiani
Chemistry Department Ugo Schiff
University of Florence
Via della Lastruccia 3, Sesto Fiorentino, 50019 Firenze, Italy

D. S. Wiersma
Physics Department
University of Florence
Via G. Sansone 1, Sesto Fiorentino, 50019 Firenze, Italy

The ORCID identification number(s) for the author(s) of this article can be found under https://doi.org/10.1002/adfm.202213162.

© 2023 The Authors. Advanced Functional Materials published by Wiley-VCH GmbH. This is an open access article under the terms of the Creative Commons Attribution License, which permits use, distribution and reproduction in any medium, provided the original work is properly cited.

DOI: 10.1002/adfm.202213162

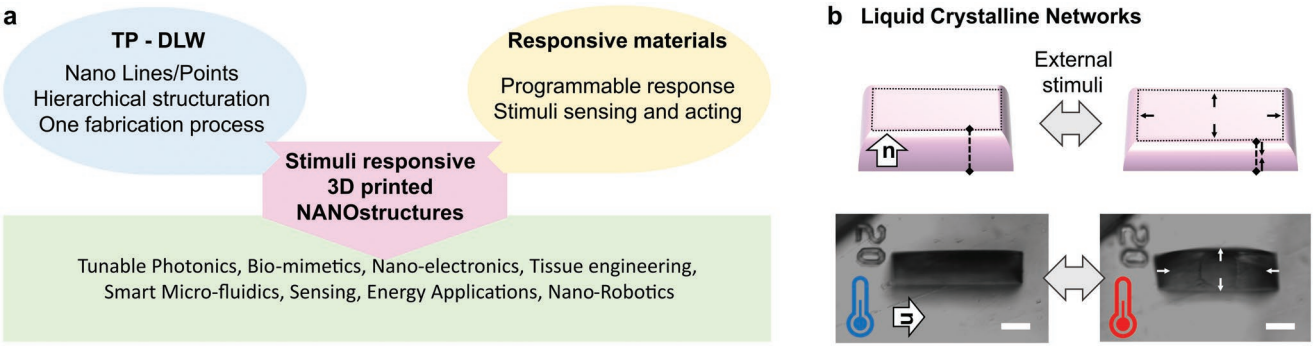

Figure 1. a) Graphic representation of the characteristics and applications of stimuli responsive 3D-printed nanostructures. b) Scheme and experimental deformation of responsive liquid crystalline networks under stimuli. Two different alignments are represented in the top scheme (homeotropic alignment) and in the bottom optical images (homogeneous planar alignment) acquired at room temperature (on the left) and under temperature actuation (on the right). The scale bar is 20 µm.

bovine serum albumin and polydimethylsiloxane micro-lenses, responsive to pH or solvent swelling,[25,26] a dye-doped bovine serum tunable micro-laser working in aqueous environment,[27] and hydrogels-based responsive photonic grating arrays with micron features.[28] Very recently, 4D microscopic photonic crystals with 100 nm resolution have been patterned for the visible range, and their structural colors have been controlled by regulating the solution pH.[29] These examples demonstrate how different responsive materials can be photopolymerized into photonic structures whose properties can be controlled by their isotropic shape change in a liquid environment. Despite the large deformation offered by hydrogel-based materials, their operation and integration are limited to a few applications because of the need of a swelling solvent. However, for practical applications, tunability should be extended to dry environments, possibly exploiting different anisotropic deformations too. These needs can be addressed by Liquid Crystalline Networks (LNCs), materials bearing the typical phase transitions of liquid crystals and the elasticity of rubbers. With respect to the other responsive polymers, LCNs present an anisotropic molecular structure where mesogens (the liquid crystalline units) are first aligned in a desired way and then polymerized to obtain a polymeric network that retains this ordered structure.[30–32] The deformation under stimuli and hence the polymer smart functionality is related to this molecular alignment that has to be carefully controlled once developing a specific device as shown in Figure 1b. During the application of selected external stimuli, a progressive disordering of the mesogenic moieties attached to the polymers is translated into a net contraction along the nematic director with an expansion in the perpendicular directions (Figure 1b). Engineering the LC alignment makes these polymeric networks able to perform specific 3D deformation using a single material and a single fabrication process.[33] Once the stimulus is removed, the materials are able to return in their original shape thanks to the crosslinked architecture.

In previous works, nematic LCNs have been patterned in micro structures for photonic applications such as 2D diffraction grating, birefringent color pixels, and whispering gallery mode resonator, whose properties have been controlled via temperature variation or light stimulus.[19,34–38] Cholesteric liquid crystals were exploited for a 3D-printed optical sensor in which humidity/temperature changes rule the resulting structural coloration.[39] Besides photonic applications, additive manufacturing of LCNs at the microscale has recently been reported for 3D mechanical metamaterial[40] and for LCN actuators responsive to temperature variation.[41] However, all the reported LCN structures, even if characterized by micrometric features, mostly in 2D geometries (e.g., gratings),[35,37] do not show sub-diffraction limited resolution and a good mechanical stability to be patterned in 3D complex design such as 3D responsive photonic crystals (PCs). The softness of deformable polymers together with the relative monomer swelling that they undergo during the printing process at room temperature inevitably introduces defects and deviations from the intended design. To increase the rigidity of the polymerized network (cross-linking degree) and therefore to improve the mechanical stability and reproducibility of soft 3D structures, higher laser powers are required that, on the other hand, strongly increases the voxel size, with a resulting detrimental effect on the resolution. To overcome these limitations, the TP-DLW technique, which offers a resolution of ≈150 nm for glassy commercial polymers, should be implemented with a temperature controlling unit of the sample in order to limit the swelling of monomers into the soft cross-linked network during the printing process. The authors have already shown that a polymerization temperature of 10 °C slows down the monomer diffusion in soft responsive materials, improving the resolution and the mechanical stability up to performances typical of commercial glassy resists.[42] Furthermore, lowering the polymerization temperature makes the polymerizable unit (the voxel) more spheroidal thus reducing the aspect ratio (i.e., the ratio among the major and minor axis of the voxel) and, last but not least, greatly improves the reproducibility of the printed structures, thus opening to the fabrication of photonic crystals able to work in dry environment.

Photonic crystals have a peculiar optical feature, the inhibition of the light propagation in a certain frequency range (stop-band for low refractive index contrast, $\Delta n < 1.9$; and complete bandgap for high refractive index) that derives from their permittivity periodicity. This property gives rise to bright structural colors and can be used to create lossless waveguides and cavities.

However, the tuning of laser-printed 3D photonic crystals in liquid environments has only recently been reported,[29] and

© 2023 The Authors. Advanced Functional Materials published by Wiley-VCH GmbH

to the best of our knowledge, the unique example reporting a TP-DLW-fabricated tunable woodpiles working in dry environment exhibits a slight refractive index tuning without reporting the relative change in the stopband.[43] Here, we report on the fabrication of a polymeric woodpile with a well-defined stop band in the near infrared range that can be reversibly tuned in response to temperature variation. During actuation, the photonic crystal characterized by a liquid crystal (LC) homeotropic alignment undergoes a reduction of the PC height and therefore of the vertical periodicity, thus enabling the modulation of the reflectivity at the telecom wavelengths.

2. Results and Discussion

2.1. Fabrication of 3D-Printed Elastic Photonic Crystals

The fabrication of the microstructures has been achieved by LCN mixture already tested for the realization of other 2D photonic structures capable to deform more than 20% of their initial length depending on the polymerization condition.[35–37,44] Two-photon polymerization has been performed at 10 °C by means of a Peltier cell and at room temperature for comparison (**Figure 2**a). In this technique, the nanometric

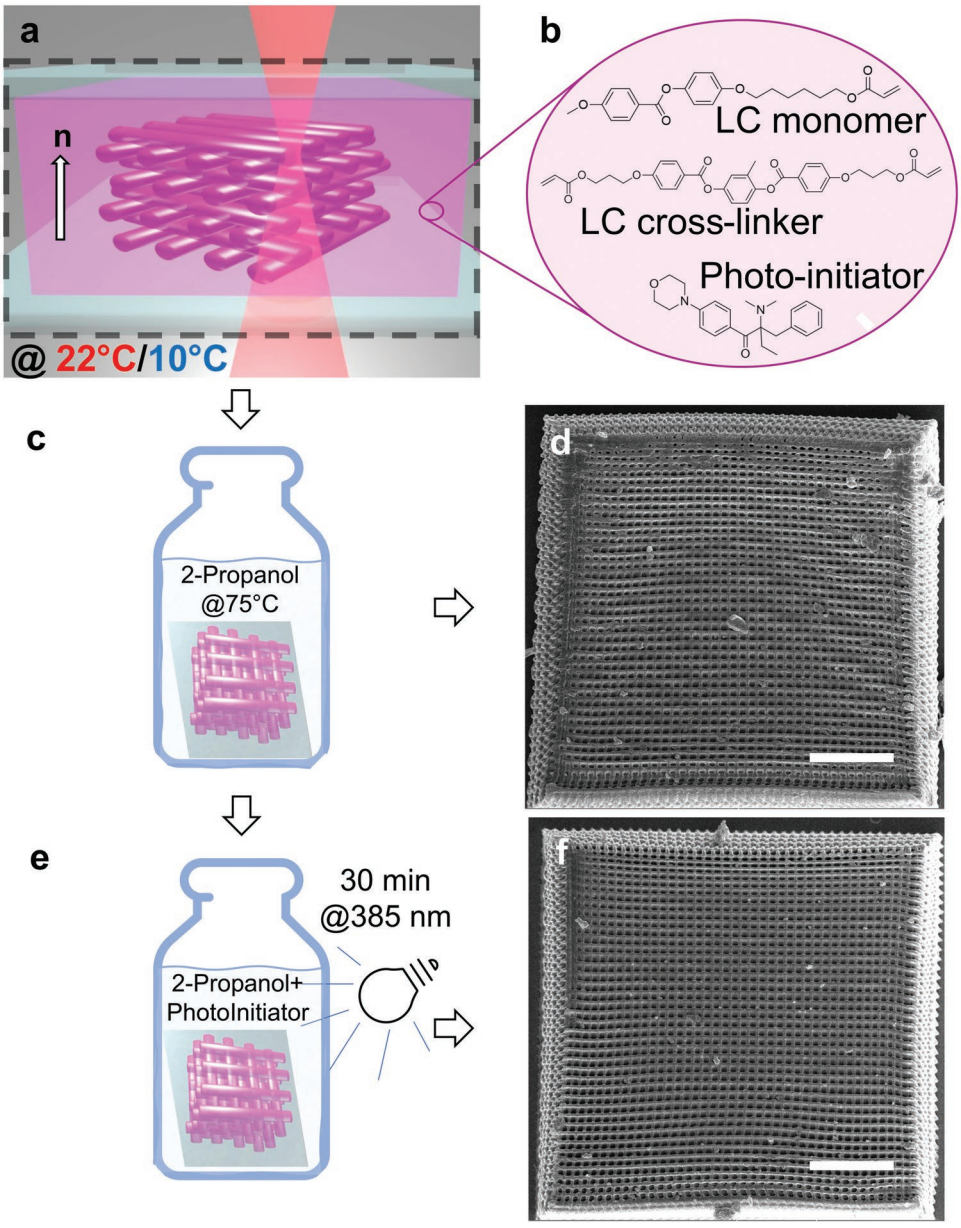

Figure 2. Fabrication of elastic woodpile photonic crystal made by LCNs. a) Scheme of the TP-DLW printing of 3D PC into a homeotropically aligned LC cell. The temperature of the mixture during printing has been controlled by a Peltier cell and fixed at 22 and 10 °C. b) Molecular composition of the liquid crystalline mixture. c) Scheme of the development process of the structure in 2-propanol at 75 °C. d) SEM image of the woodpile obtained after the fabrication step of Figure 2c. e) Scheme of the post UV curing process to complete the polymerization. f) SEM image of the woodpile obtained after the step of Figure 2e i.e. after the post-curing process. The scale bars are 10 µm.

© 2023 The Authors. Advanced Functional Materials published by Wiley-VCH GmbH

resolution is guaranteed by the activation of the radical reaction only in the focal spot where the two-photon absorption by the initiator allows for radical formation in a confined nanometric volume.

The monomeric formulation, shown in Figure 2b, is composed by a polymerizable liquid crystal mesogen (C6BP, 69% mol/mol), a liquid crystal cross-linker (RM257, 30% mol/mol), and a photo-initiator (Irgacure 369, 1% mol/mol). This formulation presents a nematic phase at room temperature (after a first melting step) and allows to achieve a good rigidity of the materials opening to the fabrication of 3D structures with nanometric suspended elements.[45] In 3D photonic crystals, the control of the frequency range of the stop band can be achieved via a mechanical contraction along the light propagation direction, perpendicular to the substrate, keeping the in-plane symmetry of the unitary cell. To satisfy such a requirement, we choose the homeotropic alignment where the LC director is perpendicular to the glass substrate (Figure 2a). A standard LC cell has been thus prepared with two glasses coated with a suitable polyimide and then infiltrated by capillarity with the melted mixture. After cooling to room temperature, a monodomain LC with homeotropic alignment is obtained and verified at the polarized optical microscope (POM).

After the polymerization, the LCN cell was developed in 2-propanol at 75 °C, in order to dissolve the unpolymerized material without any degradation of the polymerized structures (Figure 2c). Then a post curing process was performed by UV irradiation of the structure after immersion in a solution containing the photo-initiator (Figure 2e). The molecular alignment of the structure has been verified using a POM as reported in Figure S1 (Supporting Information). Figure 2d,f shows the scanning electron microscope (SEM) images of the woodpile PC before and after the UV curing step. As it can be observed, the post curing reduces the swelling of the rods that are more straight improving the constant periodicity of the diffractive structure as well as the mechanical stability.[46]

The 3D LCN woodpile is made of 16 layers (4 periods separated by a distance *d*, see **Figure 3**a for a scheme of the fabricated structure), the length of each rod is 50 µm and the in-plane periodicity (*a*, distance in between parallel rods) is 1.2 µm in the designed geometry. Among the different woodpile geometries (face-centered-cubic with $\frac{d}{a}=\sqrt{2}$, body-centered cubic, bcc, with $\frac{d}{a}=1$, or centered-tetragonal with $d/a \neq 1$), we targeted a centered-tetragonal woodpile, nearly a bcc structure ($\frac{d}{a}\approx 1$, see Figure 3a), because, for fixed filling fraction, their stop band occurs at a lower ratio of vacuum wavelength to rod spacing, *a*, than for the face-centered-cubic woodpile thus reducing the miniaturization challenge.[47] Woodpile photonic crystals have been patterned on a LCN base that should both remove the strain of the rigid glass substrate (which can reduce the deformation during actuation) and promote a more homogeneous shrinkage of the 3D structure during the development process.[48,49]

One major hurdle in the fabrication of soft photonic structures is the reproducibility of the results and the fidelity of the final structure with respect to the intended design, which was here overcome by the temperature-controlled TP-DLW[42] also leading to a more spheroidal shape of the voxel. Figure 3b,c shows two PCs printed at room temperature and 10 °C, respectively. It is evident that using a controlled polymerization temperature allows to improve the resolution and the mechanical stability of the PC, also reducing the defects due to the polymer swelling (effect that causes the merging of some top woodpile lines in Figure 3b).

2.2. Optical Characterization of Woodpiles

The woodpile PCs have been characterized by the optical setup reported in **Figure 4**a. The transmission spectroscopy setup is constituted by a super-continuum source, linearly polarized and then selectively filtered in wavelength via an acousto-optic tunable filter (AOTF) in the range from 1300 to 1800 nm. The monocromatic light is then focused on the sample and the transmitted light is collected with a 20X objective, and imaged by a near-infrared camera, thanks to a tube lens, or focused on a photodiode to measure the spectral response. The thermal variation of the optical properties of the PCs has been controlled using a hot plate while they are optically probed by the near infrared laser.

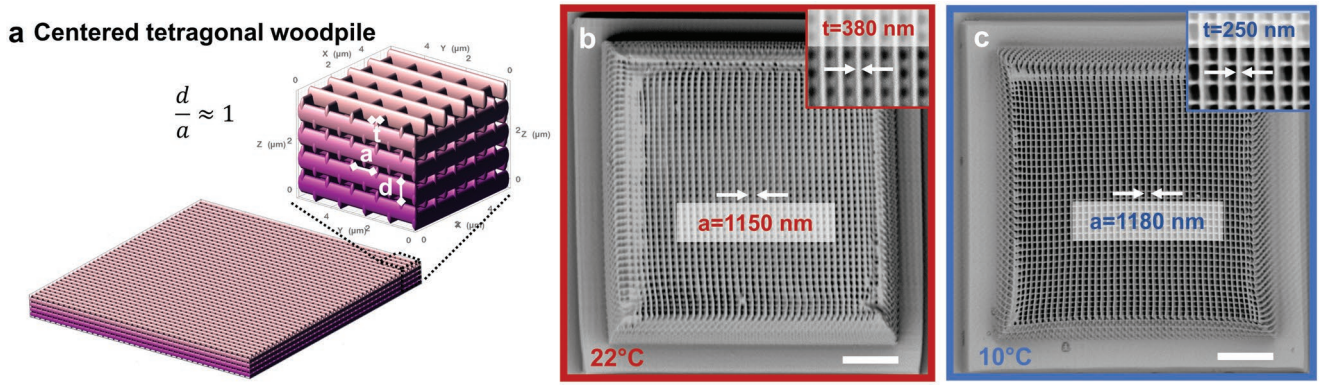

Figure 3. Woodpile design and final printed polymeric structures. a) Rendering of the woodpile PC. b,c) SEM images of the PC woodpiles printed at room temperature b) and at 10 °C c). The scale bars are 10 µm.

© 2023 The Authors. Advanced Functional Materials published by Wiley-VCH GmbH

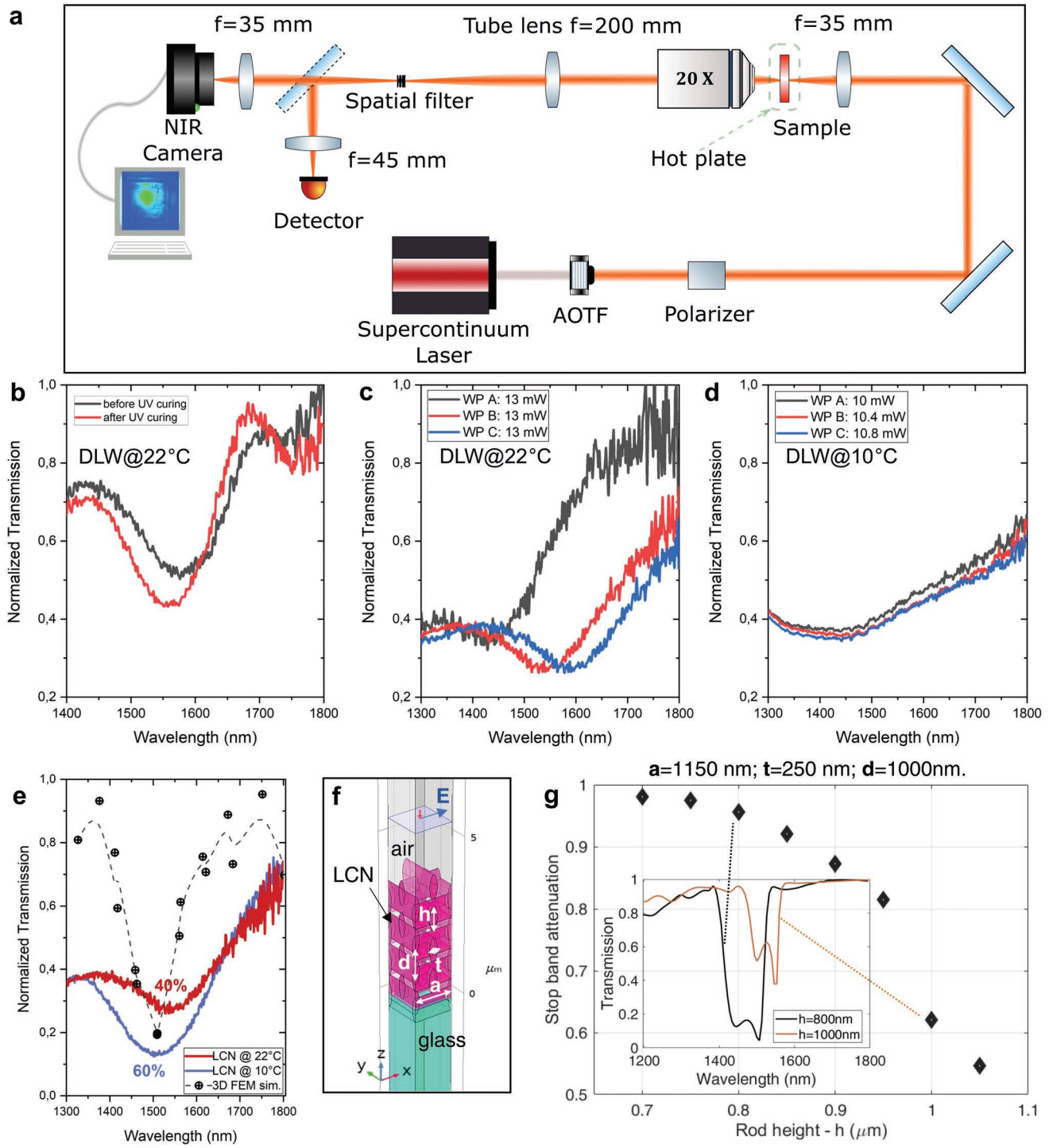

Figure 4. Optical characterization. a) Scheme of the optical setup. b) Transmittance measurement of the stop band of the woodpile obtained before (black line) and after the UV curing (red line). c) Reproducibility test for woodpile structures printed at 22 °C: structures written with the same laser power have a stop band in different frequency ranges. d) Reproducibility test for woodpile structures printed at 10 °C: structures written with slightly different laser powers show stop bands in the same frequency range. e) Transmittance measurement of the stop band of the woodpile obtained for the woodpile written at 10 °C (blue line) and room temperature (red line) compared to the transmittance spectrum calculated for a 3D PC with FEM calculation (black scatters). The FEM calculation has been performed on a PC with finite size (4 periods in the z direction and 11 μm x 11 μm x-y dimensions). f) Schematics of the periodic unit cell used for the FEM calculations reported hereafter. Parameters such as the thickness and height of the woodpile rods have been varied to match the dependence of the stop band and to be compared with the experimental data. g) Dependence of the stop band attenuation on the rod thickness (major axis of the voxel) retrieved by FEM calculations performed on the periodic unitary cell. In the inset, the calculated transmittance for two different thicknesses (indicated as h in panel c).

© 2023 The Authors. Advanced Functional Materials published by Wiley-VCH GmbH

The first characterization of the elastic woodpiles was performed to monitor the effect of the post-curing on the optical properties. In Figure 4b, the transmission spectra of the same woodpile before (black spectrum) and after (red spectrum) the post-UV curing process are reported. As expected, the treatment[46] determines a slight blueshift due to the overall reduction of the rod minor and major axis.[42] Moreover, thanks to the swelling decrease, the periodicity of the structure is improved (see Figure 2d–f), therefore producing a larger attenuation (10% reduction) of the woodpile transmission at the stop band. One major difference in the 3D printing of soft materials at different temperatures is the reproducibility of the process. This fact becomes more and more relevant when addressing optical features that are sensitive to minimal deviation in the design. The case study of a photonic crystal provides a good reproducibility test as the optical properties derive from the light interference at the periodic layers, which are sensitive to subwavelength deviations. To this end, we compare the optical transmittance of the LCN photonic crystal printed at 10 °C and at room temperature (three different structures printed at the two different temperatures are analyzed in Figure 4c,d). At room temperature, uncontrollable effects at the microscale makes it almost impossible to exactly obtain two identical stop bands from micro woodpile with nominally identical structures (set by the fabrication design and lithographic parameters), as shown in Figure 4c. On the other hand, Figure 4d reports that a polymerization process at 10 °C leads to photonic structures with stop bands with negligible differences even if printed with laser powers that slightly differ. The proposed fabrication process therefore guarantees a good reproducibility and fidelity to the intended design also for small detuning of the laser power that might be induced for example to temperature changes in the fabrication laboratory.

Figure 4e shows the best transmission spectra for the PC printed at room temperature and at 10 °C. The transmittance attenuation at 1500 nm reaches 60% with a net improvement of 20% with respect to the woodpile printed at 22 °C, effectively indicating that more spheroidal voxels achieved by low temperature polymerization improve the stop band attenuation. A closer look at the SEM pictures of the WP printed at 10 °C (Figure 3c; Figure S2, Supporting Information) reveals that the stacked layers are only partially overlapped, thus originating a periodic (and not continuous bulky) structure with a periodicity in the *xy* plane of 1.15 µm (instead of 1.2 µm) because of the shrinkage. Those parameters experimentally determined by the SEM picture have been fed into the numerical calculations. Finite element method allows modeling complex 3D structures also introducing optical birefringence in periodic structures and anisotropic ellipsoidal shapes. Indeed, the ellipsoidal rods that compose the woodpile can be efficiently discretized using the tetrahedral mesh employed in FEM calculations to compute the electromagnetic fields.

The model of the computed structure exploits some measured parameters such as the rod thickness (t), xy plane periodicity (a), and refractive index (ordinary and extraordinary indices)[30] and allows to retrieve values of the rod height (h) and the overall transmittance/reflectance of the woodpiles. In particular, a calculation of a 3D PC with finite size (4 periods in the z direction and 11 µm x 11 µm x-y dimensions, see Figure S3, Supporting Information) has been performed to be compared with the experimental transmittance spectrum (Figure 4e). The computed stop band is consistent with the experimental results and their differences regarding the bandwidth and attenuation may be attributed to the shrinkage of the printed woodpile (see Figure 3b,c). Due to the extensive computational time of such a large 3D cell, all the other calculations presented hereafter have been performed considering a periodic unitary cell that mimics an infinite woodpile structure in the x-y plane. In this case, the FEM calculation results provide ideal transmission that does not take into account the finite size of the woodpile. Deviations from the experimental and numerical results can therefore be attributed to this difference together with fabrication defects.

The geometry of the unitary cell and the mesh used in the FEM calculations are reported in Figure 4f and Figure S4 (Supporting Information), respectively. By comparing the transmittance spectra of the simulated woodpile (Figure S5, Supporting Information) with the experimental results (Figure 4e) for different vertical pitches of the woodpile ($d \approx a$), the first order stop band is obtained for a unit cell vertical pitch (d) of ≈1 µm, with an average attenuation at the stop band of 90%. Furthermore, we prove that the attenuation improvement for the structure polymerized at 10 °C is effectively due to the aspect ratio reduction. For an average laser power of ≈10 mW, the voxel aspect ratio reduction from 5 to 3 corresponds to a voxel height that is reduced from 1 µm to 800 nm. Indeed, the calculated stop band attenuation decreases when considering woodpile rods with larger thicknesses (Figure 4g). The relative transmittance spectrum maps are reported in Figure S6 (Supporting Information) together with the spectra dependence on the minor axis of the ellipsoidal rods (Figure S7, Supporting Information). The more spheroidal shape of the woodpile rods leads to an increasing refractive index contrast and a resulting increase of transmission attenuation at the stop band (inset of Figure 4g). We can find the same trend both in the experimental and calculated values of the spectra that show how thicker rods determine a less effective reflection because of the reduction of the size of the air voids and a slight red shift induced by the larger effective refractive index.

2.3. Temperature Dependent Response of Elastic Woodpiles

The temperature responsivity of LCNs allows to tune the optical properties of the PC and in particular to reversibly red/blueshift the stop band by heating/cooling the structure. According to literature, increasing the temperature leads to a gradual disappearance of the LC alignment with an increasing deformation of the whole material in a wide range of temperatures.[50,51] For acrylate-based LCNs, a clear liquid crystal to isotropic phase transition cannot be accurately defined since the materials change their birefringence during heating but without completely losing it also at high temperature.[52] Thus, accurately modulating the stimulus (e.g., the temperature), a multistate material shape is obtained starting from the same actuator as reported in **Figure 5**a,b thus opening to multiple functionalities of the same device. The progressive increase of temperature can indeed be exploited to tune the photonic properties of the PC in two different regimes allowing to obtain a tunable

© 2023 The Authors. Advanced Functional Materials published by Wiley-VCH GmbH

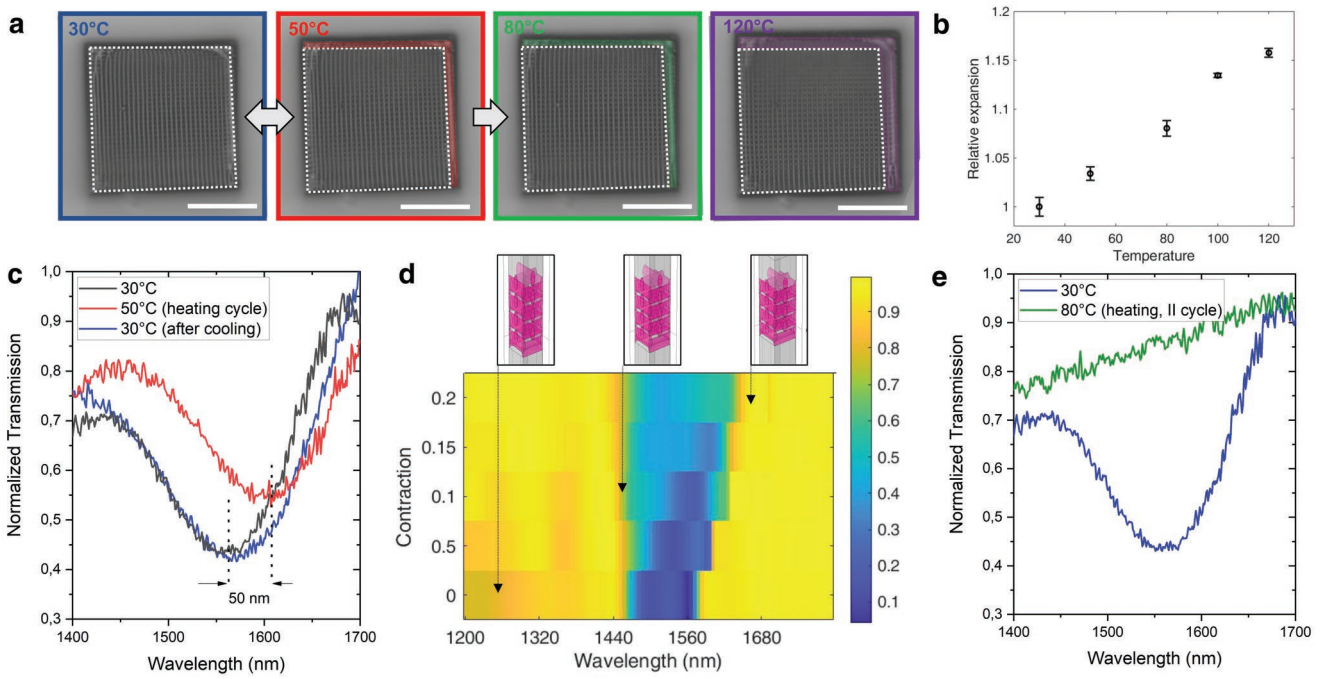

Figure 5. Temperature tuning of the PC stop band. a) Optical images of the woodpile at different temperatures. The increasing deformation with temperature is highlighted with colors (white square indicates the original shape). b) Relative expansion dependence on temperature. The estimation of the expansion (ratio of the final and initial area of the woodpile surface) and its relative error (calculated as the mean squared error from three different measurements) are retrieved from the deformations observed at different temperatures. c) Transmission spectra of the PC woodpile at room temperature (black line). By heating the structure at 50 °C, the stop band red shifts (red line) and reversibly blueshifts when cooling down to room temperature (blue line). d) Map of the calculated transmittance of the woodpile for different contraction factors whose effect is shown in the PC unit cell on the left sketches. e) Irreversible PC tuning after heating the structure above 80 °C.

photonic stop band up to a certain temperature or to irreversibly lose the photonic properties above a temperature threshold.

Figure 5c shows the stop band red shift of 50 nm when increasing the temperature of the woodpile from room temperature to 50 °C, and how the original transmission spectrum can be fully recovered when cooling it down to 30 °C. At the same time, under heating, the transmittance is reduced by 15% due to the decrease of the size of the air voids within the woodpile layers.

The temporal dynamics of the temperature modulation of the stop band is ruled by the experimental capabilities of the heating/cooling system rather than the material properties. The material response of micro and nanostructured LCNs is in the sub-millisecond regime as it has been previously measured under light activation of dye-doped formulations.[35,44] In that case, the significantly faster response is achieved by exploiting the photo-thermal activation of azo-dye doped micro-structured LCNs by remote light activation.

Looking for the physical reason that can induce the reversible shift of the stop band, two are possible major motivations that could be recognized: the refractive index variation with temperature of the nematic LCN and/or the structure deformation. In the temperature range between 30 and 50 °C, both the extraordinary and ordinary refractive index variations are negligible,[53] and even considering larger temperature ranges (up to 100 °C) a minimal variation of the ordinary refractive index would limit the red shift of the stop band to ≈5 nm (Figure S8, Supporting Information). FEM calculations allowed us to estimate the structure contraction (reported in Figure 5a,b) that actually causes the band shift. In the calculations, both the contraction and the expansion in the perpendicular plane have been taken into account keeping the total volume of the woodpile constant. Figure 5d reports the resulting red shift of the stop band when considering an increasing contraction along the LC director. A contraction of the 5% of the woodpile total height is already sufficient to determine a 50 nm red shift accompanied with a reduced transmission attenuation at the stop band. The numerical trend is in good agreement with the experimental data as in both cases the stop band undergoes a red shift together with a decrease in the attenuation and a widening of the band that becomes more and more remarkable when increasing the contraction factor.

According to FEM calculation, a contraction of the 20% would decrease the attenuation of the 50% that for the real microstructures may provoke the deletion of the measured stop band. Indeed, when the temperature of the woodpile is further increased during the transmission measurement (see Figure 5e for temperature response up to 80 °C), the stop band undergoes a bigger variation and totally flattens out. Interestingly in this case, the stop band cannot be modified in a reversible manner and the transmission spectra remain flat even once cooled down to room temperature. The irreversibility of this process may be attributed to the smaller rod separation in case of contraction larger than 5% that makes the woodpile structure more packed in the vertical direction. In the presence of some defects in the rods, this may lead to some regions that

© 2023 The Authors. Advanced Functional Materials published by Wiley-VCH GmbH

get in contact and are not more able to separate apart once the stimulus is removed due to the stickiness and softness of the material, especially at this length scale (where Van der Wall adhesion forces are dominant). Interestingly, this property can be exploited for an optical sensor with memory of the exceeding of a threshold temperature. Such temperature can be modulated by playing on the polymer composition to obtain an optical micrometric tag to monitor, for example, correct conservation of a goods.

3. Conclusion

Elastic woodpile PCs based on LCNs have been fabricated with a stop band for the telecom range taking advantage of the TP-DLW. The unprecedented, achieved resolution in soft photonic materials and good spatial periodicity of the 3D photonic crystals were successfully obtained, thanks to an optimized printing process that guarantees the reproducibility of the fabrication process and the fidelity to the design. The responsive woodpile shows an attenuation of 60% at the stop band that can be tuned of 50 nm with a slight temperature variation. By comparing experimental and calculation results, we confirm that the reversible tuning of the stop band is associated with an elastic deformation of the PC geometry associated with the environmental changes. The control obtained over the optical properties of 3D printed PCs can be used in future studies for the realization of deterministic point or line defects that can either be incorporated in the initial printing process or reversibly induced by a local light stimulus and that cannot be otherwise introduced in photonic structures based on a self-assembly process such as opal PCs.

An even more advanced perspective in light responsive elastic structures would be the "writing and erasing" of structural defects in 3D PCs exploiting the local deformation of shape changing materials. We believe that this first demonstration of nanopatterned 4D photonic crystals can further enlarge temperature and light tunability of nanophotonic devices, also exploring anisotropic birefringent materials.

4. Experimental Section

Liquid Crystalline Mixture: The preparation of the LCN mixture requires three components: a polymerizable mesogen (C6BPP), responsible of the material alignment, a cross-linker (RM257), which allows the formation of a network with an elastic mechanic response, and a photo-initiator (Irgacure 369), to achieve the spatial control of the radical polymerization reaction. In particular, the mixture contains: 69 % mol/mol of monomer, 30 % mol/mol of cross-linker, and 1 % mol/mol of initiator Irgacure 369. Monomer and cross-linker were purchased from Synthon Chemical (SYNTHON Chemicals GmbH & Co. KG, Wolfen, Germany), initiator Irgacure 369 was purchased from Sigma–Aldrich (Sigma Aldrich SRL, Milano, Italy). The choice of the mesogens, responsible for the properties of the photoresist, has been done to have a nematic phase at room temperature for several hours, making the structuration easy with the TP-DLW lithographic platform.

Cell Preparation: Homeotropically aligned LCN cells (with the director perpendicular to the glass surface) were made of two glasses both coated with PI1211 (Nissan Chemical) and separated by 20 µm spherical spacers. The LCN mixture was melted in the isotropic phase on a hot plate at 75 °C and infiltrated for capillarity. Afterward, the cell was cooled down to room temperature at −1 °C min^{-1}, and the liquid crystalline alignment was checked with a polarized optical microscope (Zeiss, Axio Observer A1, Jena, Germany). The cell was glued into a proper holder and fixed on the inverted microscope of the DLW system.

DLW Sample Printing: The 3D printing of the photonic crystal was accomplished by using the commercial platform Nanoscribe. The liquid monomer mixture enclosed in a glass cell is printed with a 100X oil immersion objective. The polymerization process of the liquid resin is induced by a nonlinear process based on a two photon absorption. In more detail, the photoinitiator added to the mixture enhances the two photon absorption of the 780 nm laser thus forming a radical. The reactive photoinitiator radical attacks C=C double bonds to produce a new C−C single bond and another radical species. The new radical species then continues the process growing the polymer chain, which continues until two radical species react, terminating the process. As a result of this process, single nano ellipsoids (defined as voxels) can be printed in sequence originating the final 3D polymeric microstructures. The presence of multifunctional molecules (cross-linkers) allows to obtain structures that were not soluble as the monomer in organic solvents thus allowing the removal of the unpolymerized part after the writing step with a development bath. The writing parameters optimized for the PC printing are a writing speed of 90 µm s^{-1} and an average laser power of ≈10–12 mW. The polymerization temperature had been monitored via a Peltier cell coupled to the LCN cell and printing process at 22 and 10 °C have been explored.[42] After the writing process, the LCN cell was removed from the sample holder, opened with a blade, and put in two development baths of 2-propanol at 75 °C, for 20 and 10 min, respectively, in order to dissolve the unpolymerized material without any degradation of the polymerized structures. After the development bath, the final polymeric structures, insoluble in the chosen solvents, remain on the glass substrate surrounded by air.

Post UV Curing: The UV curing step was performed by immersion of the printed structures into 12 mL of 2-propanol and 50 mg of photoinitiator (Irgacure 369) and irradiation with a UV lamp for 30 min. Finally, the glass slide with the woodpile structure was once more gently dipped into clean iso-propanol and air-dried.

Optical Setup: The transmission spectroscopy setup is constituted by a super-continuum source (Fianium Whitelase supercontinuum laser SC-400-4) linearly polarized through a high damage threshold polarizing cube beam splitter. An AOTF is used to rapidly and dynamically select a specific wavelength from the broadband laser source in the range from 1300 to 1800 nm. The monocromatic light (band width ≈1 nm) is then focused on the sample with a lens doublet for the infrared with a focal length of 35 mm. The transmitted light is collected with a long working distance objective 20X (Mitutoyo Plan Apo NIR Infinity Corrected Objective). A tube lens with a focal length of 200 mm focalizes the image in a back focal plane, in that a spatial filter is placed in order to collect only the k vectors perpendicular to the substrate. A flipping mirror allows deviating the beam on a near-infrared camera (Indigo Phoenix) in order to individuate the woodpile to be analyzed with a defocused laser light and put the focused spot in the middle of the chosen structure. Once aligned the sample, the transmitted light is collected by an InGaAs photo-diode (Hamamatsu G12182). A chopper in combination with a lock-in is used to eliminate the noise. The thermal actuation of the photonic structures had been attained by placing the microstructures inside a Mettler Toledo SH82 hot stage, with the cell plate facing the laser source perpendicular to the infrared laser beam.

FEM Calculation: Finite element method calculations were chosen to model the woodpile response. The choice with respect to the other common methods for electromagnetic wave propagation computation (e.g., finite difference time domain, rigorous coupled wave analysis) was dictated by the possibility to exactly reproduce the fabricated geometry made by rods with an ellipsoidal shape. Other methods based on squared grid spatial discretization would require an extremely fine mesh to well approximate the ellipsoidal shape of the rods that would result in over consumption of the memory and time consuming calculations. FEM calculations were done using the commercial software

© 2023 The Authors. Advanced Functional Materials published by Wiley-VCH GmbH

Comsol Multiphysics (RadioFrequency module, Electromagnetic Waves, Frequency Domain interface).

Two types of FEM calculations were performed: i) a 3D cell reproducing the finite size of the woodpile and ii) a unitary cell with periodic boundary conditions that reproduce a photonic structure with infinite lateral size. The first one allowed to estimate the effect of the finite size on the transmission/ reflection properties while the second one (fast computation) gave access to the contribution of the geometrical and optical properties over the resulting optical properties of the PC.

Supporting Information

Supporting Information is available from the Wiley Online Library or from the author.

Acknowledgements

This research received fundings from Fondazione Cassa di Risparmio di Firenze (2020/1583 and 2018/1047). The authors thank MIUR-Italy ("Progetto Dipartimenti di Eccellenza 2018–2022" allocated to the Department of Chemistry "Ugo Schiff"). The authors also thank Dr. Giuseppe E. Lio for his support with finite element method based calculations.

Open access funding provided by Istituto Nazionale di Ricerca Metrologica within the CRUI-CARE agreement.

Conflict of Interest

The authors declare no conflict of interest.

Data Availability Statement

The data that support the findings of this study are available from the corresponding author upon reasonable request.

Keywords

4D photonic crystals, direct laser writing, liquid crystalline networks, temperature tuning, woodpiles

Received: November 11, 2022
Revised: February 16, 2023
Published online: March 9, 2023

[1] C. A. Spiegel, M. Hippler, A. Münchinger, M. Bastmeyer, C. Barner-Kowollik, M. Wegener, E. Blasco, *Adv. Funct. Mater.* **2020**, *30*, 1907615.
[2] D. Jin, Q. Chen, T. Y. Huang, J. Huang, L. Zhang, H. Duan, *Mater. Today* **2020**, *32*, 19.
[3] D. Martella, S. Nocentini, C. Parmeggiani, D. S. Wiersma, *Adv. Mater. Technol.* **2019**, *4*, 1800571.
[4] Z.-L. Wu, Y.-N. Qi, X.-J. Yin, X. Yang, C.-M. Chen, J.-Y. Yu, J.-C. Yu, Y.-M. Lin, F. Hui, P.-L. Liu, Y.-X. Liang, Y. Zhang, M.-S. Zhao, *Polymers* **2019**, *11*, 553.
[5] Q. Li, A. P. H. J. Schenning, T. J. Bunning, *Adv. Opt. Mater.* **2019**, *7*, 1901160.
[6] M. del Pozo, J. A. H. P. Sol, A. P. H. J. Schenning, M. G. Debije, *Adv. Mater.* **2022**, *34*, 2104390.
[7] Z. Huang, G. C.-P. Tsui, Y. Deng, C.-Y. Tang, *Nanotechnol. Rev.* **2020**, *9*, 1118.
[8] B. S. Calin, I. A. Paun, *Int. J. Mol. Sci.* **2022**, *23*, 14270.
[9] V. Harish, D. Tewari, M. Gaur, A. B. Yadav, S. Swaroop, M. Bechelany, A. Barhoum, *Nanomaterials* **2022**, *12*, 457.
[10] J. Chen, A. Zhou, Y. Nie, K. Chen, Y. Zhang, Y. Xu, D. Kong, K. Shao, X. Ning, *Nano Lett.* **2022**, *22*, 135.
[11] L. Wang, Q. Li, *Adv. Funct. Mater.* **2016**, *26*, 10.
[12] T. Jeon, D.-H. Kim, S.-G. Park, *Adv. Mater. Interfaces* **2018**, *5*, 1800330.
[13] B. Tian, J. Liu, T. Dvir, L. Jin, J. H. Tsui, Q. Qing, Z. Suo, R. Langer, D. S. Kohane, C. M. Lieber, *Nat. Mater.* **2012**, *11*, 986.
[14] S. Kee, P. Zhang, J. Travas-Sejdic, *Polym. Chem.* **2020**, *11*, 4530.
[15] C. Hu, S. Pané, B. J. Nelson, *Soft Micro Nanorob.* **2018**, *1*, 53.
[16] H. Zeng, P. Wasylczyk, D. S. Wiersma, A. Priimagi, *Adv. Mater.* **2018**, *30*, 1870174.
[17] X.-Z. Chen, B. Jang, D. Ahmed, C. Hu, C. de Marco, M. Hoop, F. Mushtaq, B. J. Nelson, S. Pané, *Adv. Mater.* **2018**, *30*, 1705061.
[18] S. Nocentini, C. Parmeggiani, D. Martella, D. S. Wiersma, *Adv. Opt. Mater.* **2018**, *6*, 1800207.
[19] S. Nocentini, D. Martella, C. Parmeggiani, D. S. Wiersma, *Adv. Opt. Mater.* **2019**, *7*, 1900156.
[20] C. I. Aguirre, E. Reguera, A. Stein, *Adv. Funct. Mater.* **2010**, *20*, 2565.
[21] S. G. Romanov, A. Regensburger, A. v. Korovin, A. S. Romanova, U. Peschel, *Phys. Rev. B Phys.* **2013**, *88*, 125418.
[22] S. Kubo, Z. Z. Gu, K. Takahashi, A. Fujishima, H. Segawa, O. Sato, *J. Am. Chem. Soc.* **2004**, *126*, 8314.
[23] C. Zhou, Y. Qi, S. Zhang, W. Niu, S. Wu, W. Ma, B. Tang, *ACS Appl. Mater. Interfaces* **2021**, *13*, 26384.
[24] L. Nucara, V. Piazza, F. Greco, V. Robbiano, V. Cappello, M. Gemmi, F. Cacialli, V. Mattoli, *ACS Appl. Mater. Interfaces* **2017**, *9*, 4818.
[25] Y. L. Sun, W. F. Dong, R. Z. Yang, X. Meng, L. Zhang, Q. D. Chen, H. B. Sun, *Angew. Chem., Int. Ed.* **2012**, *51*, 1558.
[26] D. X. Lu, Y. L. Zhang, D. D. Han, H. Wang, H. Xia, Q. D. Chen, H. Ding, H. B. Sun, *J. Mater. Chem. C* **2015**, *3*, 1751.
[27] Y. L. Sun, Z. S. Hou, S. M. Sun, B. Y. Zheng, J. F. Ku, W. F. Dong, Q. D. Chen, H. B. Sun, *Sci. Rep.* **2015**, *5*, 12852.
[28] C. Delaney, J. Qian, X. Zhang, R. Potyrailo, A. L. Bradley, L. Florea, *J. Mater. Chem. C* **2021**, *9*, 11674.
[29] B. Liu, B. Dong, C. Xin, C. Chen, L. Zhang, D. Wang, J. Chu, *Small* **2022**, *19*, 2204630.
[30] T. J. White, D. J. Broer, *Nat. Mater.* **2015**, *14*, 1087.
[31] C. Ohm, M. Brehmer, R. Zentel, *Adv. Mater.* **2010**, *22*, 3366.
[32] R. S. Kularatne, H. Kim, J. M. Boothby, T. H. Ware, *J. Polym. Sci., Part B: Polym. Phys.* **2017**, *55*, 395.
[33] D. Liu, D. J. Broer, *Langmuir* **2014**, *30*, 13499.
[34] H. Zeng, D. Martella, P. Wasylczyk, G. Cerretti, J. C. G. Lavocat, C. H. Ho, C. Parmeggiani, D. S. Wiersma, *Adv. Mater.* **2014**, *26*, 2319.
[35] S. Nocentini, D. Martella, C. Parmeggiani, S. Zanotto, D. S. Wiersma, *Adv. Opt. Mater.* **2018**, *6*, 1870059.
[36] S. Nocentini, F. Riboli, M. Burresi, D. Martella, C. Parmeggiani, D. S. Wiersma, *ACS Photon.* **2018**, *5*, 3222.
[37] S. Zanotto, F. Sgrignuoli, S. Nocentini, D. Martella, C. Parmeggiani, D. S. Wiersma, *Appl. Phys. Lett.* **2019**, *114*, 201103
[38] Y. Guo, H. Shahsavan, M. Sitti, *Adv. Mater.* **2020**, *32*, 2002753.
[39] M. del Pozo, C. Delaney, C. W. M. Bastiaansen, D. Diamond, A. P. H. J. Schenning, L. Florea, *ACS Nano* **2020**, *14*, 9832.
[40] A. Münchinger, L. Y. Hsu, F. Fürniß, E. Blasco, M. Wegener, *Mater. Today Bio.* **2022**, *59*, 9.
[41] M. del Pozo, C. Delaney, M. Pilz da Cunha, M. G. Debije, L. Florea, A. P. H. J. Schenning, *Small Struct.* **2022**, *3*, 2100158.

© 2023 The Authors. Advanced Functional Materials published by Wiley-VCH GmbH

[42] I. de Bellis, S. Nocentini, M. G. Delli Santi, D. Martella, C. Parmeggiani, S. Zanotto, D. S. Wiersma, *Laser Photon. Rev.* **2021**, *15*, 2100090.
[43] Y. Hu, B. T. Miles, Y. L. D. Ho, M. P. C. Taverne, L. Chen, H. Gersen, J. G. Rarity, C. F. J. Faul, *Adv. Opt. Mater.* **2017**, *5*, 1600458.
[44] D. Martella, S. Nocentini, C. Parmeggiani, D. S. Wiersma, *Faraday Discuss.* **2020**, *223*, 216.
[45] S. Nocentini, D. Martella, C. Parmeggiani, D. S. Wiersma, *Materials* **2016**, *9*, 525.
[46] J. S. Oakdale, J. Ye, W. L. Smith, J. Biener, *Opt. Express* **2016**, *24*, 27077.
[47] I. Staude, M. Thiel, S. Essig, C. Wolff, K. Busch, G. von Freymann, M. Wegener, *Opt. Lett.* **2010**, *35*, 1094.
[48] A. Ovsianikov, J. Viertl, B. Chichkov, M. Oubaha, B. MacCraith, I. Sakellari, A. Giakoumaki, D. Gray, M. Vamvakaki, M. Farsari, C. Fotakis, *ACS Nano* **2008**, *2*, 2257.
[49] M. Renner, G. von Freymann, *Adv. Opt. Mater.* **2014**, *2*, 226.
[50] A. L. Elias, K. D. Harris, C. W. M. Bastiaansen, D. J. Broer, M. J. Brett, *J. Mater. Chem.* **2006**, *16*, 2903.
[51] G. N. Mol, K. D. Harris, C. W. Bastiaansen, D. J. Broer, *Adv. Funct. Mater.* **2005**, *15*, 1155.
[52] D. Martella, D. Antonioli, S. Nocentini, D. S. Wiersma, G. Galli, M. Laus, C. Parmeggiani, *RSC Adv.* **2017**, *7*, 19940.
[53] I. de Bellis, D. Martella, C. Parmeggiani, E. Pugliese, M. Locatelli, R. Meucci, D. S. Wiersma, S. Nocentini, *J. Phys. Chem. C* **2019**, *123*, 26522.

© 2023 The Authors. Advanced Functional Materials published by Wiley-VCH GmbH